

Analysis of the Microstructure and Thermal Shock Resistance of Laser Glazed Nanostructured Zirconia TBCs

Hui Chen, Yunfei Hao, Hongying Wang, and Weijie Tang

(Submitted April 17, 2009; in revised form June 4, 2009)

Nanostructured zirconia thermal barrier coatings (TBCs) have been prepared by atmospheric plasma spraying using the reconstituted nanosized yttria partially stabilized zirconia powder. Field emission scanning electron microscope was applied to examine the microstructure of the resulting TBCs. The results showed that the TBCs exhibited a unique, complex structure including nonmelted or partially melted nanosized particles and columnar grains. A CO₂ continuous wave laser beam has been applied to laser glaze the nanostructured zirconia TBCs. The effect of laser energy density on the microstructure and thermal shock resistance of the as-glazed coatings has been systematically investigated. SEM observation indicated that the microstructure of the as-glazed coatings was very different from the microstructure of the as-sprayed nanostructured TBCs. It changed from single columnar grain to a combination of columnar grains in the fracture surface and equiaxed grains on the surface with increasing laser energy density. Thermal shock resistance tests have showed that laser glazing can double the lifetime of TBCs. The failure of the as-glazed coatings was mainly due to the thermal stress caused by the thermal expansion coefficient mismatch between the ceramic coat and metallic substrate.

Keywords laser glazing, microstructure, nanostructured zirconia TBCs, thermal shock resistance

1. Introduction

The two main reasons for the failure of the thermal barrier coatings (TBCs) are: (i) the thermal expansion coefficient mismatch between the ceramic top coat and the metallic substrate during the thermal cycling; (ii) the growth of thermal growth oxidation (TGO) (Ref 1, 2). Compared to the conventional TBCs, the nanostructured TBCs possess relatively better thermal shock resistance due to the presence of microcrack, fine pore size (lower than 10 μm), and nanosized grains which can effectively release the thermal stress (Ref 3, 4). However, the thermal shock resistance of the nanostructured TBCs should be improved extensively for them to be used in industry. Laser glazing as an advanced processing technique has been used to modify TBCs surface. Research has shown that laser glazing can decrease the surface roughness and eliminate the porosity to densify the coatings, which are desired properties of TBCs (Ref 5, 6). Laser glazing is a promising process for improving the thermal shock resistance of the TBCs. Recently, extensive research has been

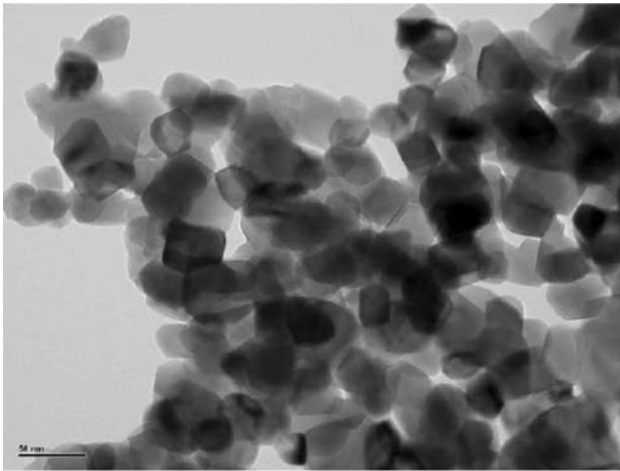
focused on laser glazing zirconia TBCs; however, the as-sprayed zirconia TBCs used for laser glazing were mainly prepared using conventional zirconia starting powder with the grain size of several tens of micron (Ref 5, 7). Therefore, the interest is in laser glazing the zirconia TBCs using the nanostructured zirconia agglomerated powders to effectively improve the performance of the TBCs. The microstructure of the as-glazed coatings has been widely investigated (Ref 5, 8, 9), but the thermal shock resistance of the laser glazed TBCs has not been fully understood up to now. The main purpose of this paper is to carry out a systematic research on the microstructure and thermal shock resistance of the laser glazed of nanostructured zirconia TBCs.

2. Experimental Details

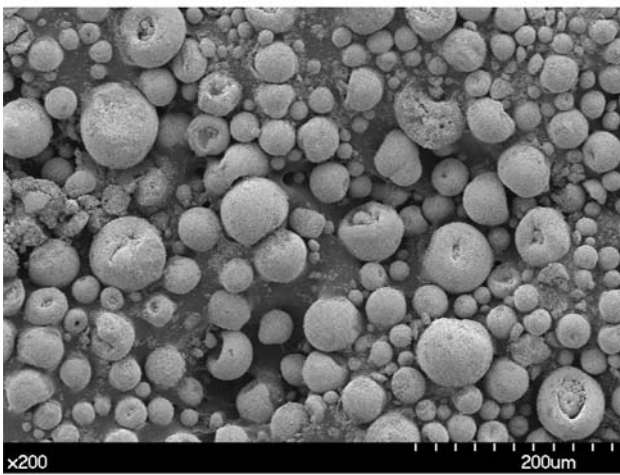
2.1 Materials

The nanostructured TBC system had a layered structure consisting of a ceramic top coat and a metallic bond coat. The ceramic top coat with the thickness ranging from 200 to 300 μm was prepared using nanostructured yttria partially stabilized zirconia agglomerated powders supplied by WUHAN Research Institute of Materials Protection. The nanostructured yttria partially stabilized zirconia powders were synthesized using the co-precipitation method and then reconstituted into spherical and near-spherical micrometer-sized granules by spray drying process before plasma spraying. Figure 1 illustrated the TEM micrograph of nanostructured zirconia particles and field emission scanning electron microscope (FESEM)

Hui Chen and Yunfei Hao, School of Materials Science and Engineering, Southwest Jiaotong University, Chengdu 610031, China; and Hongying Wang and Weijie Tang, Industrial Center, Shenzhen Polytechnic, Shenzhen 518055, China. Contact e-mail: xnrpt@swjtu.edu.cn.



(a)



(b)

Fig. 1 TEM micrograph of nanostructured zirconia particles (a) and FESEM morphology of nanostructured zirconia agglomerated powders (b)

morphology of nanostructured zirconia agglomerated powders. Figure 1(a) reveals that the size of nanostructured zirconia particles ranges from 20 to 40 nm. It can be seen from Fig. 1(b) that the agglomerated powders are spherical with the size in range of 20-80 μm . The metallic bond coat with the thickness of 80 to 100 μm was produced using NiCoCrAlY powder. The substrate material was 304 austenite stainless steel with the size of 40 mm \times 40 mm \times 6 mm. To increase the surface roughness of the substrate and improve the adhesion strength between the bond coat and substrate, the substrate was sand-blasted firstly and then ultrasonicated by supersonic with acetone.

2.2 Plasma Spraying Nanostructured Zirconia TBCs

The APS-2000 atmospheric plasma spraying (APS) equipment with the PQ-1J plasma gun was selected to prepare the nanostructured zirconia TBCs, and the detailed plasma spraying system was shown in Fig. 2.

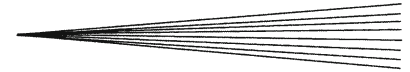


Fig. 2 Photo of the plasma spraying system

Table 1 Orthogonal design of zirconia spraying process parameters

Factors levels	Current I , A	Ar gas flow Q_1 , L min^{-1}	H ₂ gas flow Q_2 , L min^{-1}	Distance D , mm
1	500	40	4	80
2	550	45	6	100
3	600	50	8	120

During the plasma spraying process, the compressed air was used to cool the surface of the coatings. It is known that APS is a complex process with a lot of influencing factors impacting the microstructure and properties of coatings. Based on the previous research, the relatively optimum processing parameters of preparing the nanostructured zirconia TBCs were obtained through the orthogonal experiments which took thermal shock resistance of nanostructured zirconia TBCs as measurement index. In the orthogonal experiment, four main processing parameters including current, Ar gas flow, H₂ gas flow, and spraying distance were selected as experimental factors. According to the L₉(3⁴) orthogonal design table, the detailed orthogonal design of zirconia spraying process parameters was illustrated in Table 1. It must be pointed out that the thermal shock resistance of the nanostructured zirconia TBCs was tested in accordance with Chinese aviation industry standards HB7236-95 with the experimental temperature of 1000 °C.

2.3 Laser Glazing and Characterization

Laser glazing process was accomplished using a CO₂ continuous wave laser beam with the wavelength of 10.6 μm . The laser with the Gaussian distribution was operated in a TEM₁₀ mode. The laser beam with the diameter of 5.08 mm was focused on the nanostructured TBCs surface, and the power of the laser beam was 315 W. The laser scanning velocity was adjusted from 50 to 300 mm/min to control the surface figuration of the as-glazed coatings. During the laser glazing, the 99.999% Ar gas was used for cooling and protecting the coating surface. Laser glazing processing parameters are illustrated in

Table 2 Laser glazing processing parameters

Processing parameters	Laser power, W	Focal position, mm	Spot diameter, mm	Scanning velocity, mm/min	Energy density, J/mm ²	Shielding gas
LG1				300	12.40	
LG2				200	18.60	
LG3	315	+50	5.08	150	24.80	Ar
LG4				100	37.20	
LG5				75	49.61	
LG6				50	74.40	

detail in Table 2. Laser energy density was employed to evaluate the energy absorbed by unit area of coating surface at unit time when the laser beam swept across the coating surface. And the energy density can be calculated by the formula: $S = \frac{P_{\text{output}}}{VD}$, where S is the energy density; P_{output} is the power output of the continuous wave laser beam; V is the scanning velocity of the laser beam; and D is the diameter of the laser spot localized on the surface of the coating.

To evaluate and compare the thermal shock behavior of the as-sprayed and as-glazed coatings, the thermal shock test was carried out according to the standard of HB7236-95. Therefore, the tested coatings were heated in a furnace for 10 min at 1000 °C and then dropped into the water of 293 K. When a visible TBC exfoliation area reached about 5% of the total area, the test was stopped and the number of thermal shock cycles for each specimen was recorded.

XRD was applied to determine the phase composition of the as-glazed coatings before and after thermal shock failure. The surface and fracture morphology of the as-glazed coatings before and after thermal shock failure were performed using the JSM-5910LV scanning electron microscope. And the cross-sectional micrographs of the nanostructured TBCs were examined using the Hitachi S-4700 FESEM. The nanostructured zirconia particles were observed with the H-800 transmission electron microscope (TEM).

3. Results and Discussion

3.1 Optimization of Preparing the Nanostructured TBCs

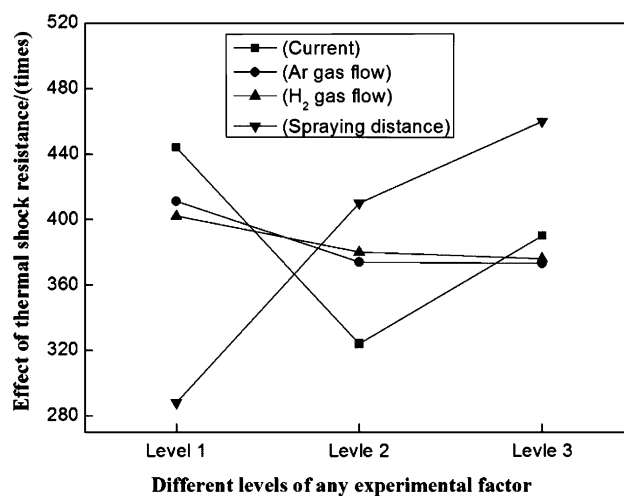
Results of orthogonal experiments for preparing the nanostructured zirconia TBCs were shown in Table 3. As can be seen from Table 3, the nanostructured zirconia TBCs exhibited the best thermal shock resistance with the thermal shock cycles of 165 when the current was 500 A, Ar gas flow rate was 50 L/min, H₂ gas flow rate was 8 L/min, and spraying distance was 120 mm. Range analysis method was employed to analyze the results listed in Table 3, and the results of range analysis were illustrated in detail in Table 4. In the range analysis, K_i indicates the sum of experimental results when the value of any experimental factor equals to the value of level i . R is the abbreviation of range, and the value of R equals to the

Table 3 Results of orthogonal experiments for preparing the nanostructured TBCs

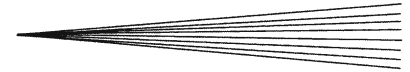
Sample	Current I , A	Ar gas flow Q_1 , L min ⁻¹	H ₂ gas flow Q_2 , L min ⁻¹	Distance D , mm	Thermal shock cycles
1	500	40	4	80	129
2	500	45	6	100	150
3	500	50	8	120	165
4	550	40	6	120	139
5	550	45	8	80	68
6	550	50	4	100	117
7	600	40	8	100	143
8	600	45	4	120	156
9	600	50	6	80	91

Table 4 Results of range analysis

	Current I , A	Ar gas flow Q_1 , L min ⁻¹	H ₂ gas flow Q_2 , L min ⁻¹	Distance D , mm
K_1	444	411	402	288
K_2	324	374	380	410
K_3	390	373	376	460
R	120	38	26	172

**Fig. 3** The factor-thermal shock resistance effect diagram

difference between the max $\{K_1, K_2, K_3\}$ and min $\{K_1, K_2, K_3\}$ in terms of any experimental factor. The higher the value of R , the larger the variation of the experimental results, and vice versa. Therefore, the value of R can be used to judge the influence of different factors on the experimental results. According to Table 4, the effect relationship diagram between the different experimental factors and the thermal shock resistance of the nanostructured TBCs was obtained as illustrated in Fig. 3. It can be seen from Table 4 and Fig. 3 that the R of current, Ar gas flow, H₂ gas flow and spraying distance was 120, 38, 26, 172, respectively. So in terms of different factors affecting the thermal shock resistance of nanostructured TBCs, the factors were as follows: spraying distance, current, Ar gas flow and H₂ gas flow, and the spraying



distance was the most important factors. This result was ascribed to the flying velocity and melting state of the agglomerated powders mainly dependent on the spraying distance. When the spraying distance was relatively shorter or longer, the spraying velocity and melting state cannot reach to the optimal state. So there existed an appropriate range of spraying distance, and the flying velocity and melting state can reach to the optimal state to improve the adhesion strength.

3.2 Microstructural Features of the As-Sprayed and As-Glazed TBCs

The cross-sectional micrographs of the nanostructured zirconia TBCs using FESEM are shown in Fig. 4. As the results indicate that, the microstructure of the as-sprayed TBCs is composed of two distinct structures. One is the fully melted area which evolved from the fully molten part

of the nanostructured zirconia agglomerated powders, as shown in Fig. 4(a). The main characteristic of this area is the columnar crystal structure. The columnar grains have grown to a few microns in the direction parallel to the crystal growth, and have been more than 100 nm in the direction perpendicular to the crystal growth. The other was the nonmelted or partially melted area which evolved from the nonmelted or partially melted part of the nanostructured zirconia agglomerated powders, as shown in Fig. 4(b). It can be seen that the morphology of this area was similar to the morphology of the starting agglomerated powders. There were many little particles with the size lower than 100 nm, and these fine grains can be used as the core of the crystallization which was beneficial to refining the grain of the zirconia TBCs. These little particles contain large volume fraction of pores with the size from several tens of nanometer to micrometer which can effectively improve the insulation property of the TBCs. So, the microstructure of the as-sprayed TBCs exhibited a unique, complex microstructure consisting of columnar grains and nonmelted or partially melted nanosized particles.

From visual inspection, the coating surface color changed from light gray to glassy transparent after laser glazing. And the main characteristics presenting in the plasma-sprayed nanostructured TBCs such as protrusions, splats, porosity, nanostructured partially melted particles and nanosized grains all disappeared after laser glazing. Compared with the as-sprayed coatings, the as-glazed coatings were densified and smooth, and the main characteristic of the surface of the as-glazed coatings was net-cracks. It must be pointed out that the net-cracks do not extend to the depth of the as-glazed coatings. In other words, the size of the net-cracks in the direction perpendicular to the surface of the as-glazed coatings is much shorter than coating thickness.

Figures 5 and 6 presented the surface and fracture morphology of as-glazed coatings with the different scanning velocity of 100 and 200 mm/min, respectively. As shown in Fig. 5, the typical microstructure of the fracture surface was fully dense columnar grain with the diameter of about 50 μm , and the representative feature of the as-glazed top surface was fine equiaxed grain with the diameter of 3-5 μm . As to Fig. 6, the coatings consisted of a single columnar microstructure both from the fracture surface and also from the as-glazed top surface micrograph. It appeared that the difference of the microstructure with the two laser glazing conditions was related to the different solidification rate under different laser energy density imported into the coatings. The lower the energy density is, the higher the thermal gradient, the shallower the melted layer, and vice versa. So, when the scanning velocity is high, the cooling rate is so rapid that the melted layer can be solidified rapidly to form the single columnar structure. Whereas with the scanning velocity decreasing, on one hand the melted layer became thicker, on the other hand the thermal conductivity of the ZrO_2 was low, so the microstructure of the coating was a combination of columnar grain in the fracture and equiaxed grain on the surface (Ref 10).

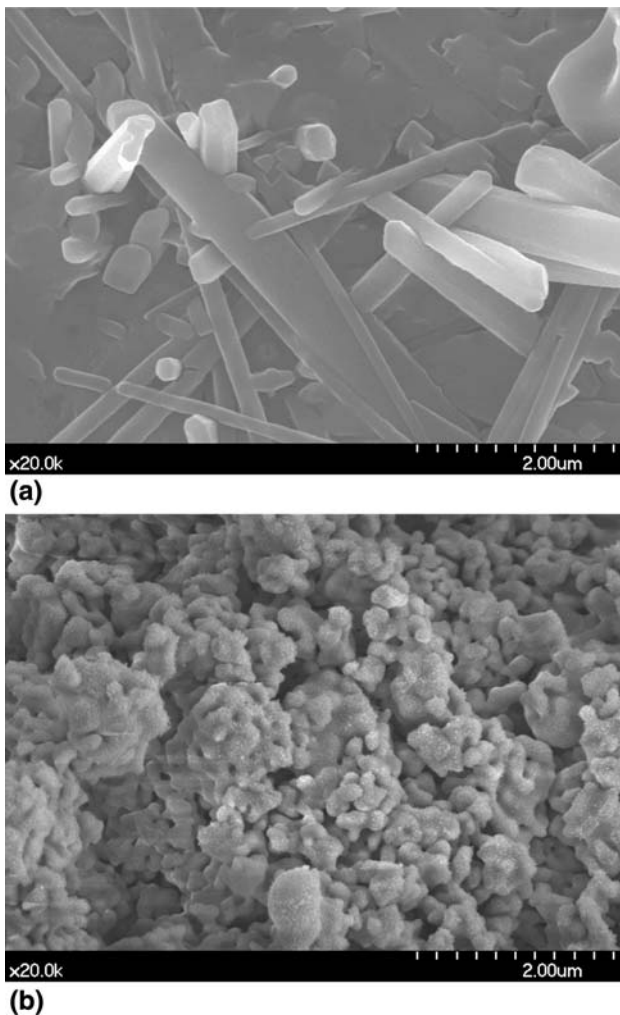
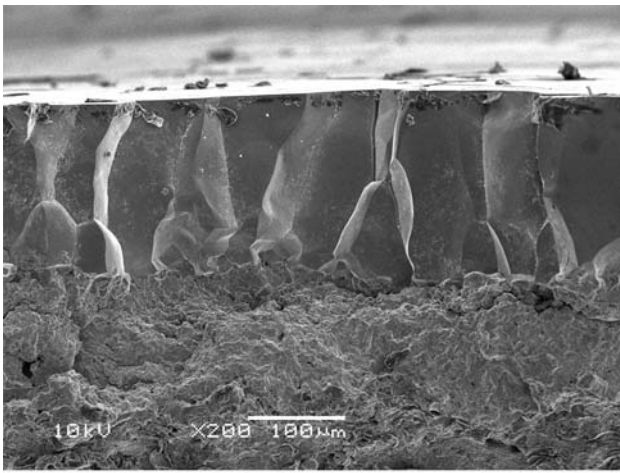
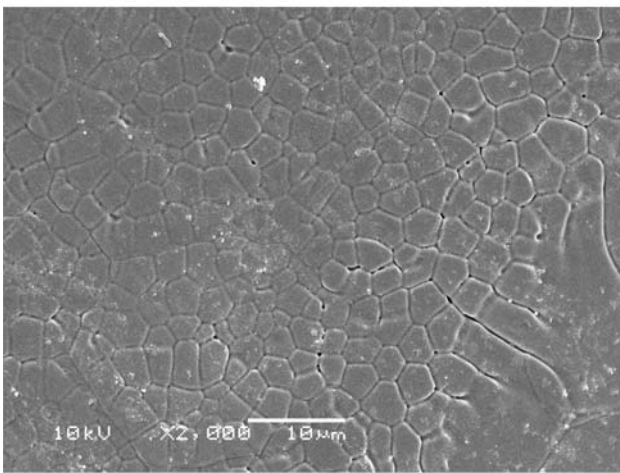


Fig. 4 FESEM micrographs of cross section of as-sprayed zirconia TBCs. (a) Columnar grains of the coatings and (b) unmelted or partially melted area of the coatings

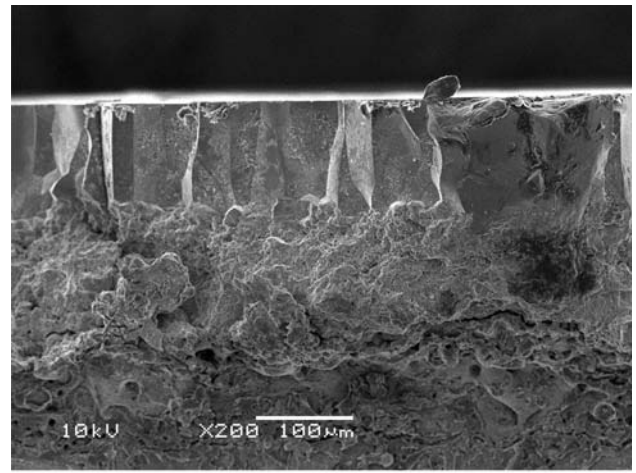


(a)

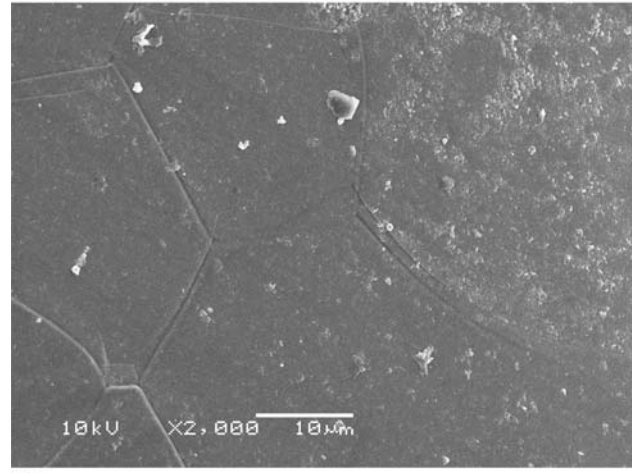


(b)

Fig. 5 Surface and fracture morphology of the as-glazed coatings with the scanning velocity of 100 mm/min; (a) fracture surface morphology and (b) as-glazed top surface morphology



(a)



(b)

Fig. 6 Surface and fracture morphology of the as-glazed coatings with the scanning velocity of 200 mm/min; (a) fracture surface morphology and (b) as-glazed top surface morphology

3.3 Structural Analysis and Phase Transformation

As shown in Fig. 7, the phase compositions of the as-sprayed and the as-glazed coatings with different laser glazing conditions were analyzed and compared. XRD analysis indicated that the predominant phase of all the coatings was the metastable tetragonal phase without the presence of monoclinic phase. This phenomenon resulted from the rapid solidification during the process of APS and laser glazing (Ref 8). It must be noted that the (220) and (400) peaks in the as-glazed coating with the scanning velocity of 200 mm/min exhibited clearly orientation, and the intensity of the (220) peak rose to the greatest. However, the other as-glazed coating did not show obvious orientation. Particularly noteworthy was that the result of XRD analysis was consistent with the result of the surface and fracture microstructure of the as-glazed coatings. The microstructure of the as-glazed coatings with the laser scanning velocity of 200 mm/min was single columnar grains, and the direction of crystal growth was

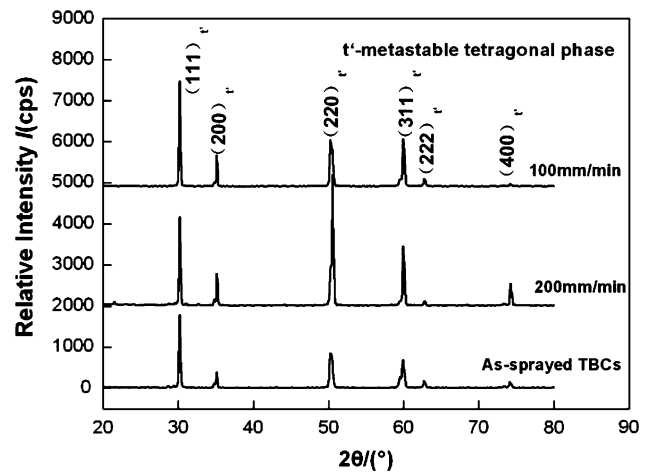


Fig. 7 Comparison of the phase composition among the as-sprayed coatings and as-glazed coatings with the different scanning velocity

perpendicular to the top surface. So the XRD pattern of the as-glazed coatings with the laser scanning velocity of 200 mm/min can show orientation. However, the microstructure of the as-glazed coatings with the laser scanning velocity of 100 mm/min was a combination of columnar grains in the fracture surface and equiaxed grains on the top surface, and the fine equiaxed grain on the top surface did not show that.

3.4 Thermal Shock Resistance of the As-Glazed Coatings

3.4.1 The Effect of Laser Energy Density on the Thermal Shock Resistance. Figure 8 displayed the effect of laser energy density on the thermal shock resistance of different laser glazed coatings. It could be seen that the as-glazed coatings exhibited different thermal shock resistance with the variation of the laser energy density. The as-glazed coating presented the best thermal shock resistance with the thermal shock cycles of 396 was about 2.4 times as large as that of nanostructured TBCs as the energy density reached 37.2 J/mm². When the energy density ranged from 12.4 to 37.2 J/mm², the thermal shock resistance of the as-glazed coatings gradually increased with the thermal shock cycles ranging from 143 to 396. While the energy density increased from 37.2 to 74.4 J/mm², the thermal shock cycles of the as-glazed coatings decreased from 396 to 115.

It should be pointed out that the thermal shock resistance of as-glazed coatings with the energy density of 12.4 and 74.4 J/mm² was lower than that of the nanostructured TBCs. This phenomenon was ascribed to the surface figuration of the as-glazed coatings. The as-glazed coating with the energy density of 12.4 J/mm² showed craters on the surface and closed pores in the fracture. As to the latter glazed coating, the main defect was surface color change which was mainly attributed to the higher energy density making the thickness of as-glazed coating exceed the top coat into the metallic bond coat.

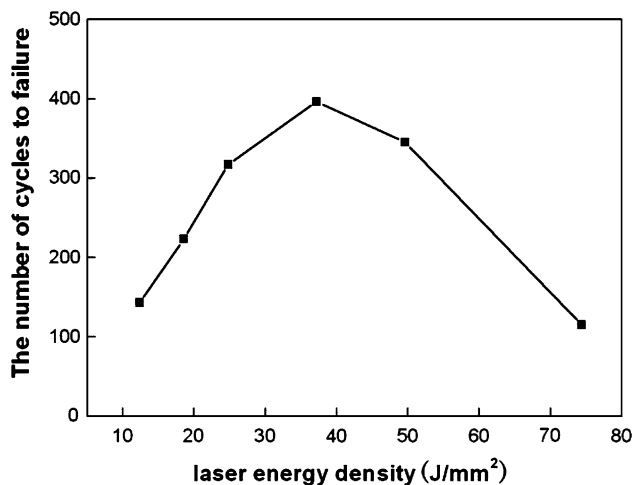


Fig. 8 The effect of laser energy density on the thermal shock resistance of different laser glazed coatings

The as-glazed coatings with the energy density ranging from 18.6 to 49.6 J/mm² all possessed better thermal shock resistance than that of nanostructured TBCs. Particularly noteworthy was that the thermal shock resistance of the glazed coating with the energy density of 37.2 and 49.6 J/mm² was better than that of the coating with the energy density of 18.6 and 24.8 J/mm². This was because the microstructure of the latter coatings was only composed of single columnar grains, while the former coating was a combination of columnar grain in the fracture and equiaxed grain on the surface. The equiaxed grain on the densified glazed coatings can effectively decrease the permeability of the high temperature corrosion medium into the bond coat. In terms of the columnar grain, there was a certain space among the columnar grains for expansion and contraction during the heating and cooling process, and so this phenomenon can eliminate the volume effect arising from the thermal stress (Ref 11). And the columnar grain can effectively reduce the thermal stress induced by the thermal expansion coefficient mismatch between the ceramic top coat and metallic substrate. The net-microcrack located on the surface of the as-glazed coatings can improve the strain tolerance and thermal shock resistance. So compared to the microstructure of the coatings consisting of the single columnar grain, the glazed coatings with a combination of columnar grains in the fracture and fine equiaxed grains on the surface possessed better thermal shock resistance. It can be concluded that the thermal shock resistance of the coatings was closely related to the microstructure and the type of defects.

3.4.2 Analysis of Phase Composition and Transformation. As illustrated in Fig. 9, the phase compositions of the as-glazed coatings with the energy density of 37.2 J/mm² before and after thermal shock failure were analyzed and compared. It can be found that the metastable tetragonal phase remained the major phase after 396 thermal shock cycles, and there was no monoclinic phase present. So the laser glazed coatings had higher

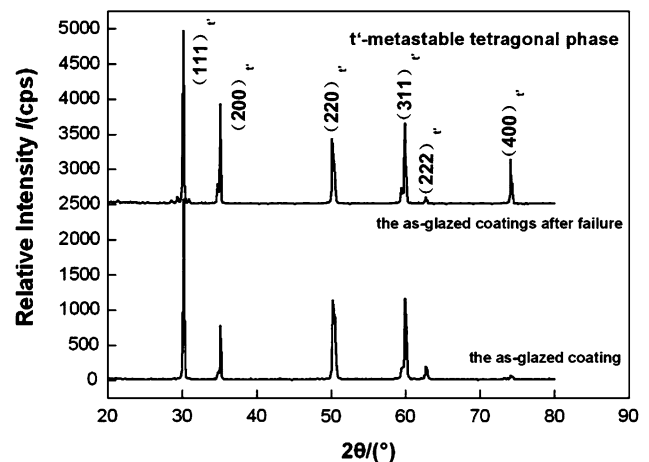


Fig. 9 Comparison of the x-ray diffraction patterns of the as-glazed coatings with the energy density of 37.2 J/mm² before and after thermal shock failure

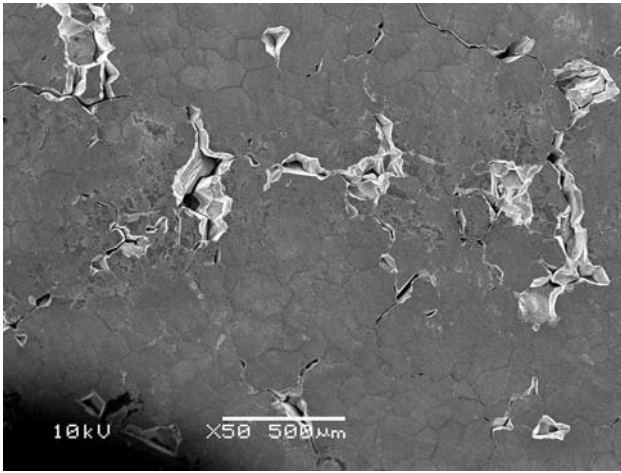


Fig. 10 Surface morphology of the laser glazed coatings after thermal shock failure at 1000 °C

phase stability during the thermal shock test. And it should be mentioned that the as-glazed coatings never bore the stress caused by the phase transformation. So it followed that the phase composition remaining the same before and after thermal shock failure was one of the reasons for the improvement of the thermal shock resistance.

3.4.3 Mechanisms. Figure 10 depicted the surface morphology of the as-glazed coatings with the energy density of 37.2 J/mm² after thermal shock failure. It could be seen that the as-glazed coatings exhibited a unique form of failure. As described above, it had been known that the main structural characteristics of the as-glazed coatings with the energy density of 37.2 J/mm² were net-microcracks, fine equiaxed grains on the surface and columnar grains in the fracture. The equiaxed grain on the surface had a limited capacity of releasing the thermal stress due to the closely accumulated structure. So the exfoliation with the size ranging from 3 to 5 μm firstly took place on the equiaxed grain. And the small unit loss became more and more with the thermal shock cycles increasing. But the columnar grain and net-microcrack had a good capacity of releasing the thermal stress, so the degradation of the coating could extend to the boundary of the columnar grain and the net-microcrack. In other words, when the exfoliation reached the border of the columnar grain and the net-microcrack, it would change to take place along the direction of the columnar grain. It should be pointed out that the exfoliation does not extend to the bond coat, even the nonglazed ceramic top coat. So the thermal stress was the main reason for the failure of the as-glazed coatings.

4. Conclusions

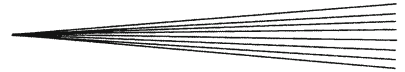
- (1) The nanostructured zirconia TBCs possessed a unique complex microstructure consisting of columnar grains and nonmelted or partially melted nanosized particles.

After laser glazing, the main features presenting in the nanostructured zirconia TBCs all disappeared, and the main characteristic of the surface of the as-glazed coating was net-cracks.

- (2) SEM examination indicated that the microstructure of the as-glazed coating can be altered from single columnar grains to a combination of columnar grains in the fracture and equiaxed grains on the surface with the variation of laser energy density.
- (3) XRD analysis showed that the predominated phase of the as-glazed coating was the metastable tetragonal phase, and the as-glazed coating with the energy density of 18.6 J/mm² had an orientation in (220) and (400) peaks. The XRD results conformed to the analysis of the microstructure of the different as-glazed coatings.
- (4) Laser energy density had an obvious effect on the thermal shock resistance of the as-glazed coatings. As the laser energy density reached 37.2 J/mm², the as-glazed coating exhibited best thermal shock resistance with the thermal shock cycles of 396 which was 2.4 times as large as that of nanostructured TBCs.
- (5) The experimental results of the thermal shock resistance indicated that the as-glazed coatings with a combination of the columnar grains in the fracture and the equiaxed grains on the surface possessed the best thermal shock resistance, and the net-microcrack, the columnar grain and the equiaxed grain were all advantageous for improving the strain compliance of the as-glazed coatings.
- (6) The thermal stress was the main reason for the failure of the as-glazed coatings.

References

1. C. Zhou, N. Wang, and H. Xu, Comparison of Thermal Cycling Behavior of Plasma-Sprayed Nanostructured and Traditional Thermal Barrier Coatings, *Mater. Sci. Eng.*, 2007, **A452-453**, p 569-574
2. B. Liang and C. Ding, Thermal Shock Resistance of Nanostructured and Conventional Zirconia Coatings Deposited by Atmospheric Plasma Spraying, *Surf. Coat. Technol.*, 2005, **197**, p 185-192
3. W.Q. Wang, C.K. Sha et al., Microstructural Feature, Thermal Shock Resistance and Isothermal Oxidation Resistance of Nanostructured Zirconia Coating, *Mater. Sci. Eng.*, 2006, **A424**, p 1-5
4. M. Gell, Application Opportunities for Nanostructured Materials and Coatings, *Mater. Sci. Eng.*, 1995, **A204**, p 246-251
5. C. Batista, A. Portinha, R.M. Ribeiro et al., Morphological and Microstructural Characterization of Laser-Glazed Plasma-Sprayed Thermal Barrier Coatings, *Surf. Coat. Technol.*, 2006, **200**, p 2929-2937
6. C. Sreedhar, G. Santhanakrishnan et al., Effect of Processing Parameters on the Laser Glazing of Plasma-Sprayed Alumina-Titania Ceramic, *J. Mater. Process. Technol.*, 2001, **114**, p 246-251
7. C. Batista, A. Portinha, R.M. Ribeiro et al., Surface Laser-Glazing of Plasma-Sprayed Thermal Barrier Coatings, *Appl. Surf. Sci.*, 2005, **247**, p 313-319
8. G. Antou, G. Montavon, F. Hlawka et al., Microstructures of Partially Stabilized Zirconia Manufactured Via Hybrid Plasma Spray Process, *Ceram. Int.*, 2005, **31**, p 611-619



9. S. Ahmaniemi, M. Vippola, P. Vuoristo et al., Modified Thick Thermal Barrier Coatings: Microstructural Characterization, *J. Eur. Ceram. Soc.*, 2004, **24**, p 2247-2258
10. B. Huang, H. Wang, Y. Hao, and W. Tang, Investigation on Surface Figuration and Microstructure of Laser Glazed Nanostructure Zirconia Thermal Barrier Coatings, *China Weld.*, 2009, **18**, p 51-56
11. J.R. Nicholls, K.J. Lawson, A. Johnstone et al., Methods to Reduce the Thermal Conductivity of EB-PVD TBCs, *Surf. Coat. Technol.*, 2002, **151-152**, p 383-391